Analysis of the forward *I-V* characteristics of Al implanted 4H-SiC p-i-n diodes with modeling of recombination and trapping effects due to intrinsic and doping-induced defect states

M. L. MEGHERBI[1], F. PEZZIMENTI[2,4], L. DEHIMI[3], A. SAADOUNE[1], and F. G. DELLA CORTE[2]

1.—Laboratory of Metallic and Semiconducting Materials, Mohammed Khieder University, 07000 Biskra, Algeria. 2.—Mediterranea University of Reggio Calabria, DIIES, 89100 Reggio Calabria, Italy. 3.—Faculty of Science, Elhadj Lakhdar University, 05000 Batna, Algeria. 4.—e-mail:fortunato.pezzimenti@unirc.it, Tel: +39 0965875274 Fax: +39 0965875463.

In this paper the impact of silicon carbide intrinsic defect states, such as $Z_{1/2}$ and $EH_{6/7}$ centers, on the forward current-voltage curves of aluminum (Al) implanted 4H-SiC p-i-n diodes is investigated by means of a physics based device simulator. During the simulations, an explicit carrier trap effect due to an electrically active defect concentration produced by the Al^{+} ion implantation process in the anode region was also taken into account. The obtained current-voltage characteristics are compared with those measured experimentally for several samples at different current levels. It is found that intrinsic defect densities as high as the epilayer doping may lead to undesirable device properties and instability of the forward bias behavior. The diode ideality factor and the series resistance increase with the increase of defects and could be controlled by using high-purity epi-wafers. Furthermore, due to their location in the bandgap and capture cross sections, the impact of $Z_{1/2}$ centers on the device electrical characteristics is more severe than that of $EH_{6/7}$ centers.

Keywords: Silicon carbide, p-i-n diode, numerical simulations, defect states, series resistance.

This is a post-peer-review, pre-copyedit version of an article published in Journal of Electronic Materials, n. 47, pp. 1414-1420, 2018. The final authenticated version is available online at: https://doi.org/10.1007/s11664-017-5916-8

INTRODUCTION

During the recent years, the 4H polytype of silicon carbide (4H-SiC) has been identified as a wide bandgap semiconductor with the potential to offer great performance improvements in power electronics [1-4]. Compared to more conventional materials, like silicon (Si) or gallium arsenide (GaAs), 4H-SiC is well known for its higher critical electric field (2-3 MV/cm), thermal conductivity (3.5-4 W/K·cm), and saturated carrier velocity (2×10^{7} cm/s) [5]. However, 4H-SiC technology still has to face important technological issues among which the presence of intrinsic material defects in large area substrates and epilayers, as well as the

control of unintentionally introduced defects by ion implantation [6-8]. In fact, the presence of defects has a strong impact on the electrical characteristics of 4H-SiC based devices and, depending on their location in the bandgap, defects act for electrons and holes both as traps and as recombination centers. Traps reduce the semiconductor free carrier density, whereas recombination centers introduce generation-recombination currents in rectifying devices [9,10]. Therefore, considering the important scattering mechanisms for which experimental or theoretical data is not quite available, intensive efforts should be made in order to gain control and understanding of defect activity.

In this paper, the electrical characteristics of aluminum (Al) implanted 4H-SiC p-i-n diodes are investigated by a numerical simulation study developed using a commercial finite-element device simulator [11]. Recombination and trapping effects due to an intrinsic defect concentration of $Z_{1/2}$ and $EH_{6/7}$ centers, and the incomplete activation of the ion-implanted impurities, are carefully taken into account. The simulated behaviors as functions of defects with both different densities and locations are compared with those measured experimentally for several diodes at various conduction regimes. By fitting the experimental results, the fundamental device electrical parameters, namely the ideality factor and series resistance, are extracted as reference values.

DEVICE DESCRIPTION

The 4H-SiC p-i-n diodes considered in this work were fabricated by the CNR Institute for Microelectronics and Microsystems – Unit of Bologna (Italy). The diodes are based on a commercially available <0001> 8° off-axis n/n$^+$ 4H-SiC epitaxial wafer having a 5-µm-thick and 3×10^{15} cm^{-3} nitrogen (N) doped epilayer as schematized in Fig. 1. The epilayer thickness and doping concentration assure a theoretical breakdown voltage on the order of 1 kV.

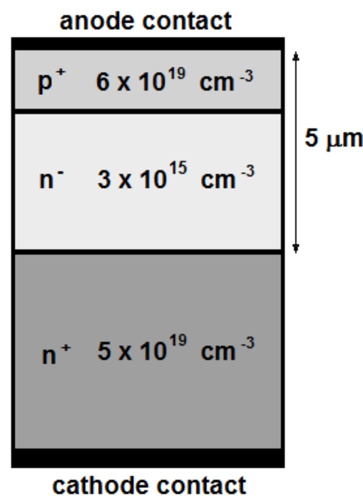

Fig. 1. 4H-SiC p-i-n diode schematic cross section. Plot not in scale.

The anode regions were realized by multiple implantation doses of Al at a temperature of 673 K. From secondary ion mass

spectroscopy (SIMS) measurements on the implanted profiles, the Al concentration is 6×10^{19} cm^{-3} up to 0.2 μm from the surface and then decreases with an half-Gaussian shape crossing the epilayer doping at 1.35 μm [12]. The anode and cathode ohmic contacts were made by deposition of titanium-aluminum (Ti-Al) dots on the p^+ implanted regions and a nickel (Ni) film on the n^+ back surface of the wafer, respectively. Further details about the adopted 4H-SiC technology, the implantation process, and the post-implantation annealing are reported in Ref. 13 and reference therein.

For all the samples the calculated active area is in the range $0.75\text{-}1\times10^{-3}$ cm^2 and the anode contact resistance is close to 1.5 mΩ·cm^2 at room temperature [13]. From the literature, this Ti-Al specific contact resistance can be considered a typical value for depositions on highly doped p-4H-SiC samples (i.e., $p \geq 2\times10^{19}$ cm^{-3}) [14].

SIMULATION MODELS

The simulation analysis was carried out using the numerical device simulator ATLAS-Silvaco [11] by solving, with the Newton's method, the Poisson's equation in the form of:

$$\varepsilon\nabla^2\psi = -q(p - n + N_D^+ - N_A^-) - Q_t \,. \quad (1)$$

Here, N_D^+ and N_A^- are the ionized impurity concentrations and Q_t is the total charge due to traps which depends upon the trap density, N_t, and its probability of occupation. This charge can be expressed in terms of the carrier thermal velocities, $v_{n,p}$, capture cross sections, $\sigma_{n,p}$, and emission rates, $e_{n,p}$, by using:

$$Q_t = qN_t\left[\frac{v_p\sigma_p + e_n}{v_p(\sigma_p + \sigma_n) + (e_n + e_p)} - \frac{v_n\sigma_n + e_p}{v_n(\sigma_p + \sigma_n) + (e_n + e_p)}\right] \quad (2)$$

where v_n = 1.9×10^5 m/s and v_p = 1.2×10^5 m/s are specific 4H-SiC constants at room temperature [15], and the emission rates for electrons and holes are calculated as a function of the difference between the trap energy level and the intrinsic Fermi level, namely E_{trap}, as follows:

$$e_n = v_n\sigma_n n_i \exp\left(\frac{E_{trap}}{kT}\right), \quad (3)$$

$$e_p = v_p\sigma_p n_i \exp\left(-\frac{E_{trap}}{kT}\right). \quad (4)$$

The others basic physical models taken into account during the simulations and their reference parameters at T = 300 K are

summarized in Table I.

Table I. Physical models and reference parameters.

Shockley Read Hall (SRH) recombination [16]	$R_{SRH} = \dfrac{pn - n_i^2}{\tau_p\left(n + n_i \exp\left(\frac{E_{trap}}{kT}\right)\right) + \tau_n\left(p + n_i \exp\left(-\frac{E_{trap}}{kT}\right)\right)}$	$n_i = 6.7\times10^{-11}$ cm^{-3}
Auger recombination [17]	$R_{Auger} = \left(C_{Ap}p + C_{An}n\right)\left(np - n_i^2\right)$	$C_{An} = 5\times10^{-31}$ cm^6/s $C_{Ap} = 2\times10^{-31}$ cm^6/s
Carrier lifetime [18,19]	$\tau_{n,p} = \dfrac{\tau_{0n,p}}{1+\left(\frac{N}{N_{n,p}^{SRH}}\right)}$	$\tau_{0n} = 500$ ns $\tau_{0p} = 100$ ns $N_{n,p}^{SRH} = 1\times10^{30}$ cm^{-3}
Incomplete ionization of impurities [20-22]	$N_{A,D}^{-,+} = N_{A,D}\left(\dfrac{-1+\sqrt{1+4g_{v,c}\frac{N_{A,D}}{N_{V,C}(T)}e^{\frac{\Delta E_{A,D}}{kT}}}}{2g_{v,c}\frac{N_{A,D}}{N_{V,C}(T)}e^{\frac{\Delta E_{A,D}}{kT}}}\right)$	$N_V = 3.29\times10^{19}$ cm^{-3} $N_C = 1.66\times10^{19}$ cm^{-3} $g_v = 4$ $g_c = 2$ $\Delta E_A = 190$ meV $\Delta E_D = 70$ meV
Bandgap energy [23]	$E_g(T) = E_{g300} + \alpha\left(\dfrac{300^2}{300+\beta} - \dfrac{T^2}{T+\beta}\right)$	$E_{g300} = 3.2$ eV $\alpha = 3.3\times10^{-4}$ eV/K $\beta = 0$
Apparent bandgap narrowing [24]	$\Delta E_{gp} = A_p\left(\dfrac{N_A^-}{10^{18}}\right)^{\frac{1}{2}} + B_p\left(\dfrac{N_A^-}{10^{18}}\right)^{\frac{1}{3}} + C_p\left(\dfrac{N_A^-}{10^{18}}\right)^{\frac{1}{4}}$ $\Delta E_{gn} = A_n\left(\dfrac{N_D^+}{10^{18}}\right)^{\frac{1}{2}} + B_n\left(\dfrac{N_D^+}{10^{18}}\right)^{\frac{1}{3}} + C_n\left(\dfrac{N_D^+}{10^{18}}\right)^{\frac{1}{4}}$	$A_p = 1.54\times10^{-3}$ $B_p = 1.3\times10^{-2}$ $C_p = 1.57\times10^{-2}$ $A_n = 1.17\times10^{-2}$ $B_n = 1.5\times10^{-2}$ $C_n = 1.9\times10^{-2}$
Carrier mobility [23,25]	$\mu_{n,p} = \mu_{0n,p}^{\min}\left(\dfrac{T}{300}\right)^{\alpha_{n,p}} + \dfrac{\mu_{0n,p}^{\max}\left(\frac{T}{300}\right)^{\beta_{n,p}} - \mu_{0n,p}^{\min}\left(\frac{T}{300}\right)^{\alpha_{n,p}}}{1+\left(\frac{T}{300}\right)^{\gamma_{n,p}}\left(\frac{N}{N_{n,p}^{crit}}\right)^{\delta_{n,p}}}$	$\mu_{0n}^{\min} = 40$ cm^2/V·s $\mu_{0p}^{\min} = 15.9$ cm^2/V·s $\mu_{0n}^{\max} = 950$ cm^2/V·s $\mu_{0p}^{\max} = 125$ cm^2/V·s $N_n^{crit} = 2\times10^{17}$ cm^{-3} $N_p^{crit} = 1.76\times10^{19}$ cm^{-3}

Here, in particular, N is the total impurity concentration for a specific device region, N_A and N_D are the substitutional p-type and n-type doping concentrations, N_V and N_C are the hole and electron density of states varying with temperature, ΔE_A and ΔE_D are the acceptor and donor energy levels, and ΔE_{gp} and ΔE_{gn} are the bandgap narrowing for the p-type and n-type regions, respectively.

Finally, for high electric fields, a carrier mobility reduction due to a carrier saturated drift velocity of 2×10^7 cm/s is considered

as described in Ref. 25.

Note that the simulation setup assumed in this work has also been used in other recent papers of ours [12,26,27] and it is supported by comparison with experimental results obtained on similar Al implanted 4H-SiC p$^+$-i-n diodes in a wide range of currents and temperatures [28,29].

EXPERIMENTAL RESULTS

The measured forward current-voltage (I_F -V_F) curves of four identical diodes placed on the same die are shown in Fig. 2 in half-log scale. The measurements were performed at room temperature by means of a HP4155 Semiconductor Parameter Analyzer imposing a compliance current of 100 mA.

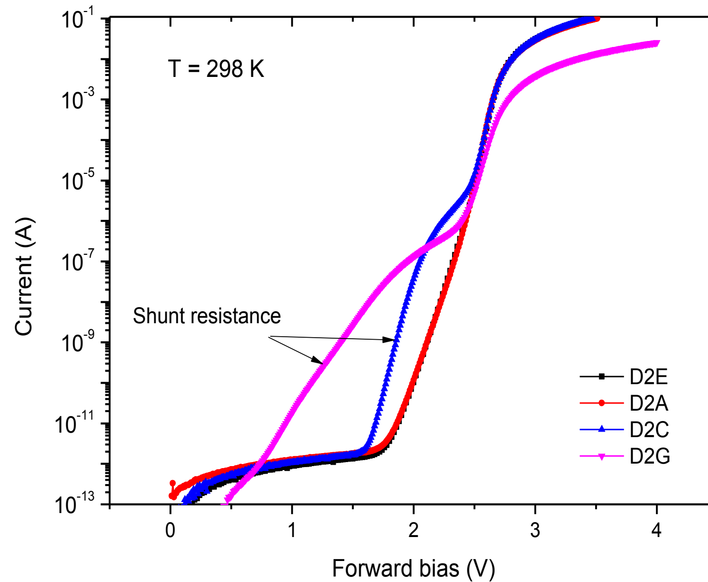

Fig. 2. Experimental I_F -V_F curves of four 4H-SiC p-i-n diodes at room temperature.

Although almost all the samples showed good rectifying behaviors with a leakage current less than 0.2 nA at -100 V, as can be observed in Fig. 2, the diodes labelled as D2C and D2G must be classified as leaky diodes. In fact, they exhibit distorted I_F -V_F characteristics (especially diode D2G) with higher currents than the well-behaved diodes D2A and D2E under low-voltage test conditions. This excess current is ascribed to an inhomogeneous epitaxial layer containing intrinsic defects that give origin to a leakage path (or a shunt resistance) connected in parallel with the actual p-i-n structure. In other words, regardless of the diode fabrication process [30,31], the leaky diode current behaviors can be modeled as due to two diodes with different barrier heights connected in parallel, each contributing to the current independently, where the defective diode has a lower turn-on voltage. Conversely, the good quality diodes D2A and D2E show the typical p-i-n electrical behavior. They are characterized by a sharp

turn-on at a threshold voltage of about 2 V and quick rise in slope, which is a characteristic of high quality and low resistance diodes. The diode current is dominated by recombination and carrier diffusion up to a bias voltage close to 2.5 V and 2.8 V, respectively. Finally, at the highest voltages, all the samples show a series resistance effect. The curves tend to become flat and the current is entirely dominated by a series resistance that can be considered as the sum of the contact contributions and the diode internal resistance. From the experimental results, a percentage on the order of 80% of the diodes was classified as well-behaved diodes.

A compact analytical current-conduction model can be written in the form of [32,33]:

$$J_{tot} = J_{Sdiff}\left[\exp\left(\frac{qV_D}{n_1 KT}\right)-1\right] + J_{Srec}\left[\exp\left(\frac{qV_D}{n_2 KT}\right)-1\right] + J_t \exp(BV_D), \quad (5)$$

where J_{tot} is the diode total current density, Js_{diff} is the saturation current density for diffusion, Js_{rec} is the saturation current density for space-charge recombination, J_t is the saturation current density for tunneling, n_1 and n_2 are ideality factors, and B is a fitting parameter. As well known, in the case of ideal diffusion $n_1 = 1$. The value of n_2, instead, is dependent on the location of recombination centers within the bandgap. Finally, the third term is attributed to shunting phenomena in order to give a better fitting of the leakage current.

By taking the natural logarithm of both sides in (5), separately in the ranges where each of the two exponential term is dominant, we obtain an expression in the form of a linear equation from which we can get the slope and, by fitting the experimental results, we have extracted the values of the diode electrical model parameters, i.e. n_1, n_2, and B, as summarized in Table II. Here, the diode series resistance, calculated by fitting the slope of the linear plot $dV_D/d\ln(J_{tot})$ vs J_{tot}, is also reported.

Table II. Diode electrical parameters.

Diode	n_1 ($2.5 < V_D \leq 2.8$ V)	n_2 ($V_D \leq 2.5$ V)	B (V^{-1})	Series resistance (Ω)
D2A	1.35	2.13	1.329×10^{-12}	7.77
D2C	1.72	3.38	1.066×10^{-12}	7.28
D2E	1.63	2.17	0.854×10^{-12}	7.32
D2G	2.03	3.53	0.997×10^{-12}	46.46

As expected, in the diffusion regime ($2.5 < V_D \leq 2.8$ V), the ideality factor can be considered in the proper value for the diodes D2A and D2E, whereas the diode D2G shows a value of n_1 strongly affected by defects resulting close to 2. In addition, in the low injection regime ($V_D \leq 2.5$ V), the diodes D2G and D2C have an ideality factor n_2 in excess of 3 as a consequence of a higher current contribution related to the recombination processes in the space-charge region.

The diode series resistance is on the order of 7 **Ω**, except for the leaky diode D2G where it appears 6 times larger. In this case, it is evident that the contribution of the series resistance related to the diode internal resistance meaningfully overcomes the contact

resistance values that we can assume to be the same for all the samples. Therefore, this result is mainly due to the lack of an effective carrier injection through the diode junction, preventing the setup of a conductivity modulation regime in the low-doped middle region.

SIMULATION ANALYSIS

By assuming the device parameters extracted from the measurements (i.e., ideality factor and series resistance) as reference values, the aim of this section is to investigate the degradation of the forward current-voltage characteristics of 4H-SiC p-i-n diodes caused by the formation of crystal defects, either as a result of interactions with energetic particles or as growth of the epitaxial layer. These defects are, in fact, deep states into the material forbidden energy gap where carriers recombine.

In accordance with the SIMS Al doping profile described above, the post-annealing residual crystal damage created by the Al^{+} ion implantation process was introduced within the diode structure in the form of a depth profile of electrically active traps up to a distance of 1.35 μm from the anode contact. In particular, considering that for implant concentrations on the order of 10^{19} cm^{-3} only a percentage close to 90% of Al atoms can be assumed to really occupy a substitutional position in the crystal [14,34,35], as an initial entry data for modeling the trap density was set, at each depth, as 10% of the implanted impurities [36]. In addition, the energy level of these traps was assumed close to the Al acceptor level, i.e. 0.2 eV from the valence band edge [21,35], determining a donor-like effect. In fact, the traps are positively charged when empty and can only capture electrons. Conversely, according to the experimental data present in literature and supported by deep-level transient spectroscopy (DLTS) measurements [30,31], the mostly two deep native defects observed in 4H-SiC based devices are in the upper half of the bandgap [14]. They are labelled as $Z_{1/2}$ and $EH_{6/7}$ and are located at 0.67 eV and 1.65 eV from the conduction band edge, respectively. These defects produce an acceptor-like effect. In other words, similarly to ionized acceptor impurities, they are negatively charged when filled and became neutral when empty.

The fundamental defect parameters assumed during the simulations are listed in Table III [14,36,37] where, for the sake of simplicity, the traps induced by the Al implantation process are labelled as $Al_{10\%}$.

Table III. Fundamental defect parameters.

Defect name	Location (eV)	Density (cm^{-3})	Electron cross section (cm^2)	Hole cross section (cm^2)
$Z_{1/2}$	0.67	$0.01\text{-}3\times10^{16}$	2×10^{-14}	3.5×10^{-14}
$EH_{6/7}$	1.65	$0.02\text{-}3\times10^{16}$	2.4×10^{-13}	1.0×10^{-15}
$Al_{10\%}$	0.2	6×10^{18} (peak value)	2.58×10^{-13}	2.58×10^{-13}

In order to describe the impact of the starting substrate on the forward current-voltage characteristics of the presented 4H-SiC p-i-n diodes, wide ranges of intrinsic defect concentrations were considered. The I_F -V_F curves obtained for three different $Z_{1/2}$ densities are shown in Fig. 3. Here, the measured characteristics of the well-behaved diode D2A and leaky diode D2C are also reported for comparison.

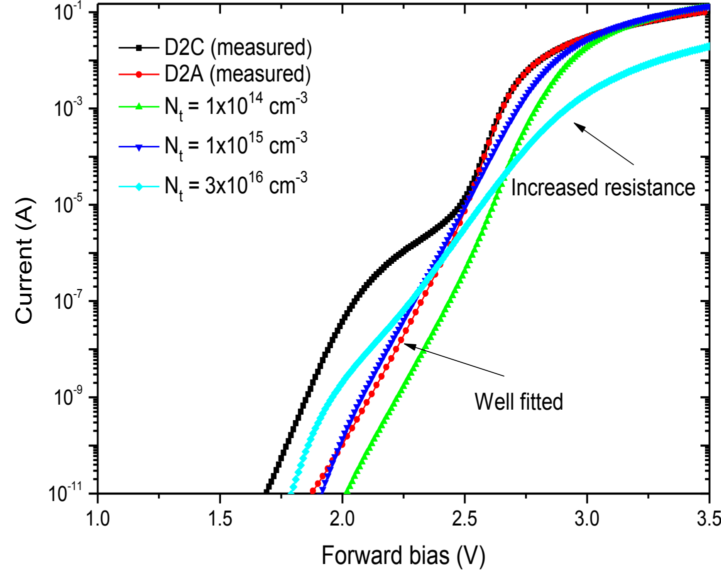

Fig. 3. Measured and simulated I_F -V_F characteristics for different $Z_{1/2}$ concentrations.

As can be seen, the $Z_{1/2}$ concentration is a key parameter that controls, at low and medium bias voltages, the parts of the forward current characteristics related to recombination and diffusion phenomena. In these regions, in fact, the diode total current is strongly influenced by the effective carrier lifetime in the epitaxial layer [38]. In particular, the carrier lifetime dependence on the trap density can be written using the standard expression [11]:

$$\tau_{n,p} = \frac{1}{v_{n,p}\sigma_{n,p}N_t} . \tag{6}$$

In Fig. 3, the curve of the diode D2A is well fitted for a $Z_{1/2}$ density of 1×10^{15} cm^{-3}. Densities exceeding the epilayer doping (e.g., $N_t = 3\times10^{16}$ cm^{-3}), however, tend to increase the shunt resistance behavior and at the same time have a detrimental effect on the diode series resistance. The main reason for this lies in the penalized flow of electrons due to defect effects, which originate in the epilayer region increasing the local recombination rate as shown in Fig. 4. Therefore, the diode current is degraded because these defects reduce the carrier lifetime and act as carrier traps in the device active region introducing high-resistive paths [39].

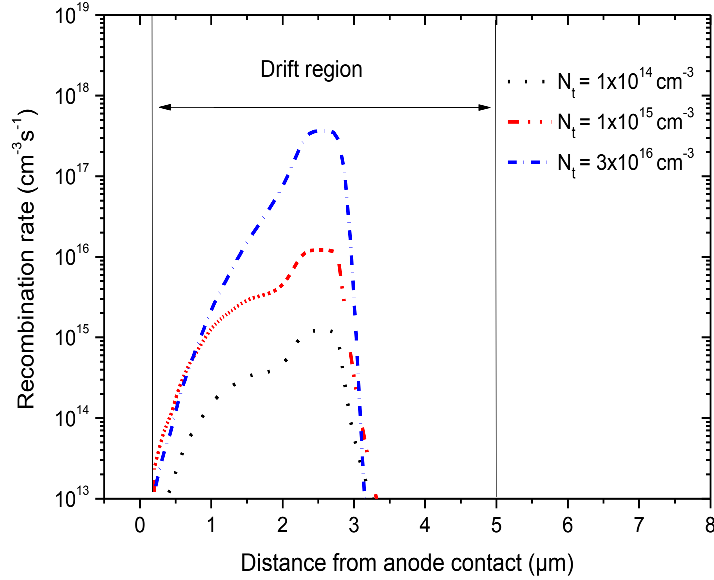

Fig. 4. Recombination rate in the drift region for different $Z_{1/2}$ concentrations. The plot was extracted by taking a vertical cut along the device axis of symmetry for $V_F = 2$ V.

The measured I_F-V_F behavior of the diode D2A and the simulated ones for different concentrations of $EH_{6/7}$ are shown in Fig. 5.

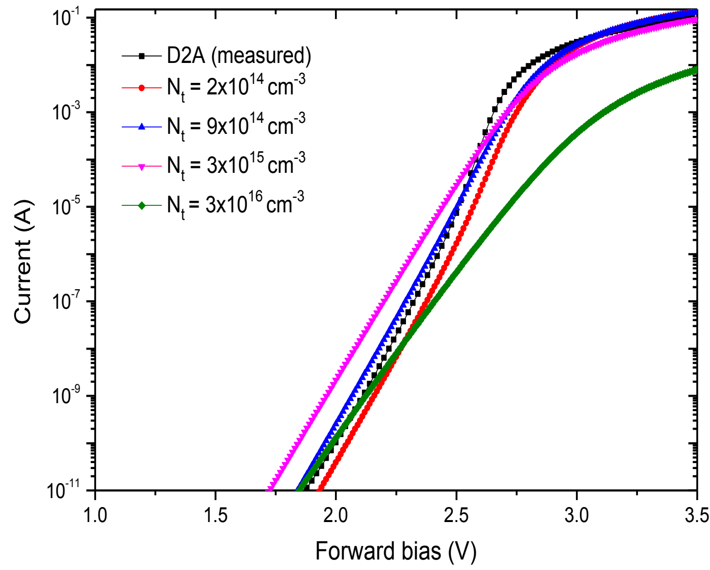

Fig. 5. Measured and simulated I_F-V_F characteristics for different $EH_{6/7}$ concentrations.

We can note that the curve of the diode D2A is rather well fitted for $EH_{6/7}$ concentrations in the upper limit of 9×10^{14} cm^{-3}. In particular, increasing N_t the linear region of the curves tends to shift toward the lower voltages and up in the whole low-medium bias

range (V_F < 2.8 V). Then, when the defect density becomes comparable to the epilayer doping (3×10^{15} cm^{-3} for our samples) it appears clear that the device electrical properties, i.e. current capability and series resistance, are heavily modified.

The changes of the diode ideality factor and series resistance for different $Z_{1/2}$ and $EH_{6/7}$ concentrations are depicted in Figs. 6 and 7, respectively.

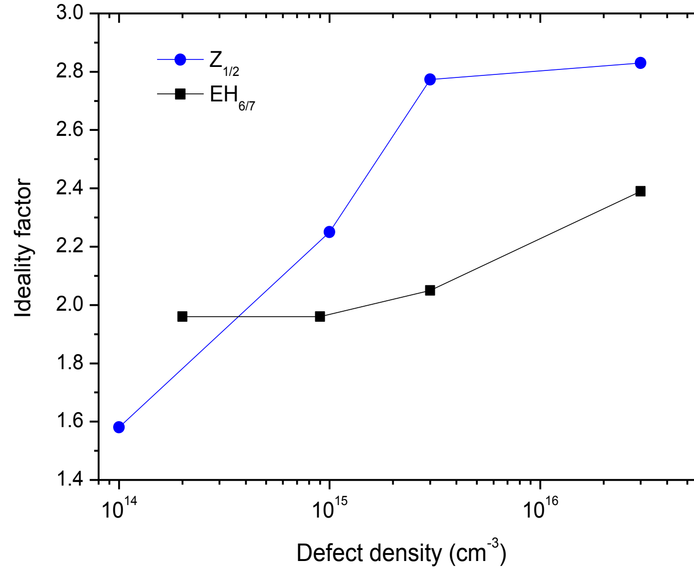

Fig. 6. Effect of different defect concentrations on the diode ideality factor calculated from the simulated I_F -V_F characteristics for $V_F \leq 2.5$ V.

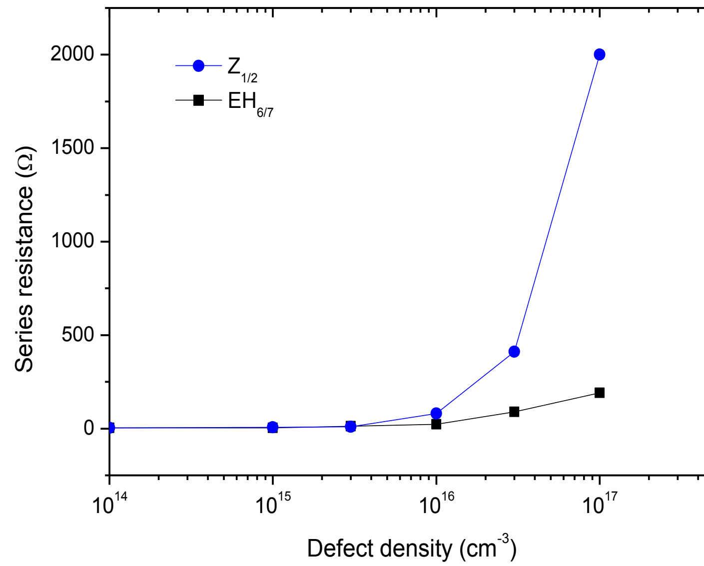

Fig. 7. Effect of different defect concentrations on the diode series resistance.

The presence of defects considerably increases the ideality factor, which is, in particular, strongly dependent on the $Z_{1/2}$ concentration. In particular, from Fig. 6 we can note that for concentrations of $Z_{1/2}$ close to 1×10^{15} cm^{-3} and $EH_{6/7}$ lower than 9×10^{14} cm^{-3}, the ideality factor agrees well with the value calculated for the good quality diodes D2A and D2E in Table II. Then, increased defect densities tend to determine ideality factors typical of leaky diodes.

On the other hand, as shown in Fig. 7, up to a defect density does not exceeding the epilayer doping ($N_t \leq 3\times10^{15}$ cm^{-3}), the series resistance is on the order of a few ohms and it appears slightly dependent on the substrate crystal quality. Then, however, the $Z_{1/2}$ concentration once again has a noticeable impact on the diode current characteristics. For example, a defect density close to 6×10^{15} cm^{-3} determines a series resistance comparable with the value calculated for the leaky diode D2G in Table II.

Finally, it is worthwhile noting that, at high forward bias voltages ($V_F > 2.8$ V), the diode series resistance is also determined by traps due to the non-substitutional Al doping concentration in the anode region, which affect, in particular, the carrier mobilities.

The simulated I_F-V_F curves for different trap concentrations set as a fraction of the implanted Al doping density are shown in Fig. 8.

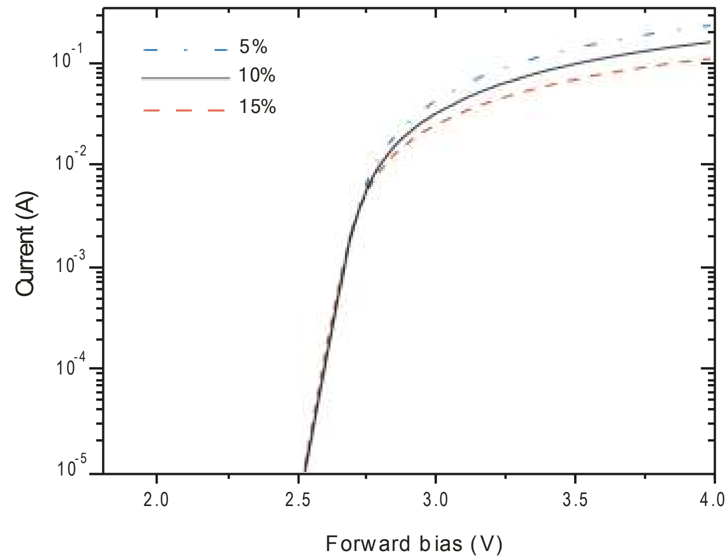

Fig. 8. Effect of different trap concentrations set as a fraction of the implanted Al doping density in the anode region.

Here, the current behaviors can be explained considering that an increased trap concentration in the anode region determines an increase of the diode internal resistance, R_i, mainly due to a decrease of the electron mobility parameter (R_i α $1/qN\mu_n$). By using the simulator to calculate the electron and hole concentration depth profiles at different bias levels, in fact, the analysis reveals that above the I_F-V_F curve knee the total diode current is dominated by the electron injection into the anode [29], resulting the concentration of free holes for conduction limited by the incomplete activation of the ion-implanted impurities. In more detail, the incomplete

ionization model predicts a saturation level of ionized acceptor concentration ~10 times lower with respect to donors and the higher dopant activated in the n^+ substrate tends to suppress the hole injection into the cathode and enhances the electron injection into the anode.

CONCLUSIONS

In this work, the forward current-voltage characteristics of Al implanted 4H-SiC p-i-n diodes have been investigated as a function of different defect states located in the material bandgap. The post-annealing residual crystal damage created by the ion implantation process has been taken into account setting in the anode region, at each depth, a trap concentration as a fraction of the chemical Al doping profile.

The presence of intrinsic defects $Z_{1/2}$ and $EH_{6/7}$ inside the epitaxial layer affects the device current behavior by varying the ideality factor from its reference value. The diode series resistance is also affected, although a significant increase, compared to the calculations extracted from the measurements, is observed only for defect concentrations exceeding the epilayer doping. The degradation of the device electrical parameters can be related to a defect activity, which determines a change in the device physics in terms of free carrier concentration, carrier lifetime and carrier mobility.

ACKNOWLEDGMENTS

The authors would like to thank R. Nipoti and the staff of the Institute for Microelectronics and systems (CNR-IMM, Bologna, Italy) for supplying the 4H-SiC diodes.

REFERENCES

[1] R. Wang, D. Boroyevich, P. Ning, Z. Wang, F. Wang, P. Mattavelli, K. Ngo, and K. Rajashekara, *IEEE Trans. Power Electron.* 28, 555 (2013).

[2] M. C. Lee and A. Q. Huang, *Solid State Electron.* 93, 27 (2014).

[3] L. Lin and J. H. Zhao, *Solid State Electron.* 86, 36 (2013).

[4] G. Calderon-Lopez, A. J. Forsyth, D. L. Gordon, and J. R. McIntosh, *IEEE Trans. Power Electron.* 29, 2474 (2014).

[5] B. J. Baliga, *Silicon Carbide Power Devices* (Singapore: World Scientific, 2005), ch. 2.

[6] K. Kawahara, M. Krieger, J. Suda, and T. Kimoto, *J. Appl. Phys.* 108, 023706 (2010).

[7] N. T. Son, X. T. Trinh, L. S. Løvlie, B. G. Svensson, K. Kawahara, J. Suda, T. Kimoto, T. Umeda, J. Isoya, T. Makino, T. Ohshima, and E. Janzén, *Phys. Rev. Lett.* 109, 187603 (2012).

[8] P. B. Klein, *J. Appl. Phys.* 103, 033702 (2008).

[9] F. Zhao, M. M. Islam, B. K. Daas, and T. S. Sudarshan, *Mater. Lett.* 64, 281 (2010).

[10] J. B. Fedison, N. Ramungul, T. P. Chow, M. Ghezzo, and J. W. Kretchmer, *IEEE Electron Dev. Lett.* 22, 130 (2001).

[11] Silvaco Atlas User's Manual, Device Simulation Software (2013).

[12] M. L. Megherbi, F. Pezzimenti, L. Dehimi, S. Rao, and F. G. Della Corte, *Solid State Electron.* 109, 12 (2015).

[13] R. Nipoti, F. Moscatelli, P. De Nicola, *IEEE Electron Dev. Lett.* 34, 966 (2013).

[14] Z. C. Feng and J. H. Zhao, Silicon Carbide: Materials, Processing and Devices (New York: Taylor & Francis, 2004), chs. 4, 5, and 6.

[15] Yu. Goldberg, M. E. Levinshtein, S. L. Rumyantsev, in *Properties of Advanced Semiconductor Materials GaN, AlN, SiC, BN, SiC, SiGe* (New York: J. Wiley & Sons, 2001), ch. 5.

[16] S. Selberherr, Analysis and Simulation of Semiconductor Devices (Wien: Springer, 1984) ch. 4.

[17] A. Galeckas, J. Linnros, V. Grivickas, U. Lindefelf, and C. Hallin, *Appl. Phys. Lett.* 7, 1:3269 (1997).

[18] P. T. Landsberg and G. S. Kousik, *J. Appl. Phys.* 56, 1696 (1984).

[19] M. Bakowski, U. Gustafsson, and U. Lindefelt, *Phys. Status Solidi A* 162, 421 (1997).

[20] M. Ruff, H. Mitlehner, and R. Helbig, *IEEE Trans. Electron Devices* 41, 1040 (1994).

[21] T. Ayalew, T. Grasse, H. Kosina, and S. Selberherr, *Mater. Science Forum* 483, 845 (2005).

[22] T. Troffer, M. Schadt, T. Frank, H. Itoh, G. Pensl, J. Heindl, H. P. Strunk, and M. Maier, *Phys. Status Solidi A* 162, 277 (1997).

[23] X. Li, Y. Luo, L. Fursin, J. H. Zhao, M. Pan, P. Alexandrov, and M. Weiner, *Solid State Electron.* 47, 233 (2003).

[24] U. Lindefeld, *J. Appl. Phys.* 84, 2628 (1998).

[25] M. Roschke and F. Schwierz, *IEEE Trans. Electron Devices* 48, 1442 (2001).

[26] F. Pezzimenti, *IEEE Trans. Electron Devices* 60, 1404 (2013).

[27] G. De Martino, F. Pezzimenti, F. G. Della Corte, G. Adinolfi, and G. Graditi, in *PRIME 2017: Proceedings of the 13th Conference on PhD Research in Microelectronics and Electronics*, (2017), pp. 221-224.

[28] F. Pezzimenti, F. G. Della Corte, and R. Nipoti, *Microelectron. J.* 39, 1594 (2008).

[29] F. G. Della Corte, F. Pezzimenti, and R. Nipoti, *Microelectron. J.* 38, 1273 (2007).

[30] W. C. Mitchela and W. D. Mitchell, *J. Appl. Phys.* 101, 053716 (2007).

[31] T. Dalibor, G. Pensl, H. Matsunami, T. Kimoto, W. J. Choyke, A. Schoner, and N. Nordell, *Phys. Status Solidi A* 162, 199 (1997).

[32] M. Wolf, G. T. Noel, and R. J. Stirn, *IEEE Trans. Electron Devices* 24, 419 (1977).

[33] S. Banerjee and W. A. Anderson, *IEEE Trans. Nucl. Science* 33, 1474 (1986).

[34] M. V. Rao, J. B. Tucker, M. C. Ridgway, O. W. Holland, N. Papanicolaou, and J. Mittereder, *J. Appl. Phys.* 86, 752 (1999).

[35] T. Troffer, M. Schadt, T. Frank, H. Itoh, G. Pensl, J. Heindl, H. P. Strunk, and M. Maier, *Physica Status Solidi* 162, 277 (1997).

[36] F. Pezzimenti, F. G. Della Corte, and R. Nipoti, in *IEEE BCTM 2009: Proceedings of the Bipolar/BiCMOS Circuits and Technology Meeting*, (2009), pp. 214-217.

[37] M. Usman, M. Nawaz, and A. Hallén, *IEEE Trans. Electron Devices* 278, 258 (2013).

[38] S. Bellone, F. G. Della Corte, L. Freda Albanese, and F. Pezzimenti, *IEEE Trans. Power Electron.* 26, 2835 (2011).

[39] C. Zaring, I. Keri, J. O. Svedberg, K. Gumaelius, M. Ostling, A. Konstantinov, M. Domeij and M. Reimark, *Mater. Science Forum* 645, 1057 (2010).